Longitudinal variations in the *F* region ionosphere and the topside ionosphere-plasmasphere: Observations and model simulations

N. M. Pedatella,[1,2] J. M. Forbes,[1] A. Maute,[3] A. D. Richmond,[3] T.-W. Fang,[4] K. M. Larson,[1] and G. Millward[4]

Received 24 February 2011; revised 19 September 2011; accepted 3 October 2011; published 7 December 2011.

[1] Constellation Observing System for Meteorology Ionosphere and Climate (COSMIC) observations of the total electron content (TEC) above and below 800 km are used to study the local time and seasonal variation of longitude structures in both the *F* region ionosphere as well as the topside ionosphere and plasmasphere. The COSMIC observations reveal the presence of distinct longitude variations in the topside ionosphere-plasmasphere TEC, and these further exhibit a seasonal and local time dependence. The predominant feature observed at all local times in the topside ionosphere-plasmasphere TEC is a substantial maximum (minimum) during Northern Hemisphere winter (summer) around 300°–360° geographic longitude. Around equinox, at a fixed local time, a wave 4 variation in longitude prevails in the daytime *F* region TEC as well as the topside ionosphere-plasmasphere TEC. The wave 4 variation in longitude persists into the nighttime in the *F* region; however, the nighttime topside ionosphere-plasmasphere TEC exhibits two maxima in longitude. The COSMIC observations clearly reveal the presence of substantial longitude variations in the *F* region and topside ionosphere-plasmasphere, and to elucidate the source of the longitude variations, results are presented based on the coupling between the Global Ionosphere Plasmasphere model and the Thermosphere Ionosphere Electrodynamics General Circulation Model. The model simulations demonstrate that the orientation of the geomagnetic field plays a fundamental role in generating significant longitude variations in the topside ionosphere-plasmasphere but does not considerably influence longitude variations in the *F* region ionosphere. The model results further confirm that nonmigrating tides are the primary mechanism for generating longitude variations in the *F* region ionosphere. The coupled model additionally demonstrates that nonmigrating tides are also of considerable importance for the generation of longitude variations in the topside ionosphere-plasmasphere TEC.

Citation: Pedatella, N. M., J. M. Forbes, A. Maute, A. D. Richmond, T.-W. Fang, K. M. Larson, and G. Millward (2011), Longitudinal variations in the *F* region ionosphere and the topside ionosphere-plasmasphere: Observations and model simulations, *J. Geophys. Res.*, *116*, A12309, doi:10.1029/2011JA016600.

1. Introduction

[2] The connection between longitudinal variations in the ionospheric *F* region and vertically propagating nonmigrating tides of tropospheric origin was first suggested by *Sagawa et al.* [2005]. A number of subsequent observational and modeling studies have clearly demonstrated the presence of longitudinal variability in various parameters such as ionospheric electron densities and total electron content (TEC), the equatorial electrojet, as well as thermosphere O/N2 ratio, density and winds [*England et al.*, 2006; *Forbes et al.*, 2009; *Hagan et al.*, 2007; *Häusler et al.*, 2010; *He et al.*, 2010; *Lin et al.*, 2007; *Lühr et al.*, 2008; *Scherliess et al.*, 2008; *Wan et al.*, 2008]. Throughout most of the year, the predominant feature of the low-latitude ionosphere, when observed at a fixed local time, is a wave number 4 (hereafter wave 4) variation in longitude and the vast majority of research has focused on this feature. The wave 4 structure in longitude exhibits a significant seasonal variation with a maximum amplitude occurring during July-October. Through comparison with the seasonal variation of different nonmigrating tide amplitudes, the wave 4 signature in the ionosphere has been attributed to the eastward propagating diurnal nonmigrating tide with zonal wave number 3 (*DE*3) [e.g., *Pancheva and Mukhtarov*, 2010; *Wan et al.*, 2008, 2010]. The wave 4 variation in the ionosphere is also observed to exhibit a phase shift of ~90°/24 h local time [e.g., *Wan et al.*, 2008]. This is the same phase shift as the

[1]Department of Aerospace Engineering Sciences, University of Colorado at Boulder, Boulder, Colorado, USA.
[2]Now at High Altitude Observatory, National Center for Atmospheric Research, Boulder, Colorado, USA.
[3]High Altitude Observatory, National Center for Atmospheric Research, Boulder, Colorado, USA.
[4]Cooperative Institute for Research in Environmental Sciences, University of Colorado at Boulder, Boulder, Colorado, USA.

0148-0227/11/2011JA016600

*DE*3 tide, providing additional evidence that the *DE*3 tide is the primary mechanism for producing the wave 4 longitude variation in the ionosphere. The connection between the *DE*3 tide and the ionosphere is further supported by the fact that the *DE*3 appears as a wave 4 variation in longitude when viewed from a fixed local time perspective.

[3] The mechanism by which the *DE*3 tide may introduce longitudinal variability into the low-latitude ionosphere is as follows. During the daytime, *DE*3 zonal winds in the ionospheric dynamo region (90–150 km) modulate the ionospheric wind dynamo which generates the low-latitude electric fields and currents [e.g., *Jin et al.*, 2008]. This results in a longitudinal modulation of the low-latitude electric field strength which in turn influences the vertical $\mathbf{E} \times \mathbf{B}$ plasma drifts that control the formation and strength of the equatorial ionization anomaly (EIA). The variations in the EIA strength with longitude result in both larger EIA crest densities and a greater latitudinal separation of the EIA crests [e.g., *Immel et al.*, 2006]. In addition to $\mathbf{E} \times \mathbf{B}$ vertical drifts, other mechanisms may contribute to the formation of the wave 4 longitude variation in the ionosphere [*England et al.*, 2010]. It should be noted that these processes are not restricted to *DE*3 and other nonmigrating tides are likely to significantly impact the low-latitude electrodynamics and ionospheric densities. This is particularly relevant during November-February when the amplitudes of other nonmigrating tides surpass that of *DE*3. The dominance of other nonmigrating tides in the ionospheric dynamo region during these time periods introduces other longitude variations such as wave 2 or wave 3 variations in longitude [e.g., *Forbes et al.*, 2008; *Pedatella et al.*, 2008]. Additionally, a number of other waves, such as stationary planetary wave 4 (*SPW*4) or the nonmigrating semidiurnal eastward propagating tide with zonal wave number 2 (*SE*2), may also contribute significantly to the observed ionospheric wave 4 longitude structure [*Hagan et al.*, 2009; *Oberheide et al.*, 2011].

[4] Since nonmigrating tides considerably influence the strength and formation of the EIA, the ionospheric signature of nonmigrating tides is most pronounced in the low-latitude *F* region [e.g., *Lin et al.*, 2007]. However, observations and modeling results have demonstrated the presence of longitude variations in the topside ionosphere [*Hartman and Heelis*, 2007; *Kil et al.*, 2008; *Ren et al.*, 2008; *Fang et al.*, 2009; *Huang et al.*, 2010; *Kakinami et al.*, 2011]. These studies have revealed the occurrence of longitude variations up to 840 km altitude. Furthermore, the longitudinal variations appear to evolve with altitude which may be related to the relative importance and differences in neutral winds, composition, and $\mathbf{E} \times \mathbf{B}$ drift in different altitude regimes. The variation in altitude of the longitude structures is particularly apparent around solstice, when the observed longitude variations in the topside ionosphere [e.g., *Huang et al.*, 2010] are significantly different than those observed at *F* region altitudes [e.g., *Pedatella et al.*, 2008; *Scherliess et al.*, 2008]. While the modulation of the EIA strength by nonmigrating tides adequately explains the presence of longitudinal variations in the *F* region, this mechanism alone may not fully explain the occurrence and structure of longitudinal variations in the topside ionosphere. In regions of large magnetic field declination, significant seasonal differences in the ion density and $\mathbf{E} \times \mathbf{B}$ drift velocity near 840 km based on measurements from the Defense Meteorological Satellites Program (DMSP) satellites are observed [*Hartman and Heelis*, 2007; *Huang et al.*, 2010]. The geomagnetic field declination is considered to play a fundamental role in generating longitude variations in the topside ionosphere. Zonal neutral winds in combination with the magnetic field declination will enhance (reduce) the vertical field-aligned wind resulting in regions of larger (smaller) ion density in the topside ionosphere [e.g., *Watanabe and Oyama*, 1996; *Huang et al.*, 2010]. *Kakinami et al.* [2011] also suggest that the meridional neutral winds may influence the longitude variations in the topside ionosphere. Meridional winds may also contribute to longitude variations in the topside ionosphere due to the displacement of the geographic and geomagnetic equators [*Su et al.*, 1996]. The seasonal variation in the winds will introduce a seasonal variation to the longitude variation in the topside ionosphere.

[5] In addition to the geomagnetic field orientation, longitudinal variations in the topside ionosphere may be connected to vertically propagating nonmigrating tides of tropospheric origin. Nonmigrating tides may introduce longitude variations in the topside ionosphere through variations in the vertical $\mathbf{E} \times \mathbf{B}$ drifts and/or scale height perturbations. Recent observations have demonstrated the existence of nonmigrating tides in thermospheric density and winds, as well as exospheric temperature [*Forbes et al.*, 2009; *Talaat and Lieberman*, 2010]. The tidal variations in exospheric temperature observed by *Forbes et al.* [2009] can influence the topside ionospheric scale height, and, in turn, ionospheric densities in the topside ionosphere. It is worth noting that the nonmigrating tides present in the thermosphere and exosphere are attributed to direct tidal penetration, and are not the result of ion-neutral coupling. This is particularly apparent for the *DE*3. Evidence for the direct penetration of the *DE*3 into the thermosphere is provided by the consistency between thermospheric observations and those predicted by Hough mode extensions (HMEs), which do not account for the day-night variations of ion-neutral coupling [e.g., *Forbes et al.*, 2009; *Oberheide et al.*, 2009]. It is, therefore, important to consider the direct penetration of the *DE*3 into the thermosphere as a mechanism for introducing longitude variations in the topside ionosphere.

[6] While past studies have demonstrated the presence of longitude variations in the topside ionosphere, the mechanisms responsible for their formation and how they compare to similar features in the *F* region remains unclear. The present study aims to further understand the longitude variations in the topside ionosphere and plasmasphere electron densities through both observations and numerical simulations. We utilize observations from the Constellation Observing System for Meteorology, Ionosphere, and Climate (COSMIC) satellites to obtain simultaneous observations of the TEC above and below 800 km altitude. This allows us to study the similarities and differences between longitude structures in the *F* region and topside ionosphere-plasmasphere along with their local time and seasonal dependencies. We further

present numerical model results which demonstrate the relative importance of nonmigrating tides and the geomagnetic field on generating longitude variations in the topside ionosphere.

2. COSMIC TEC Observations

[7] The COSMIC consists of six microsatellites and was launched in April 2006 to study the Earth's neutral atmosphere and ionosphere through the technique of GPS radio occultation. The satellites were initially launched into an orbit near 500 km altitude and over the following 17 months gradually moved into the final orbit configuration. In the final orbit, the six satellites are evenly distributed in longitude at an altitude of ~800 km and an orbital inclination of 72° [*Anthes et al.*, 2008]. In the present study we use COSMIC observations during 2008 when all of the satellites (with the exception of COSMIC-3 which is not used) were in their final orbit. The fairly even distribution in longitude combined with the local time precession of ~12 min per day make the COSMIC well suited for studying longitude and local time variations in the ionosphere. Each of the COSMIC satellites is equipped with two GPS antennae for GPS radio occultation, two GPS antennae for precise orbit determination (POD), a tiny ionospheric photometer and a triband beacon [*Rocken et al.*, 2000; *Cheng et al.*, 2006]. In the present study we use ionospheric observations of TEC from both the POD antennae and also from vertical electron density profiles obtained through the method of radio occultation. The TEC from the POD antennae provide information on electron densities above 800 km while the TEC from radio occultation provides details on the electron density up to 800 km. This method thus permits separation of the ionospheric densities into two distinct altitude regions. Further details on each of these observations are provided in the subsequent sections.

2.1. Observations of TEC Between 800 and 20200 km

[8] The quasi-zenith directed POD antennae onboard the COSMIC satellites provides information on the TEC between the COSMIC orbital altitude (~800 km) and the GPS orbital altitude (~20200 km). The TEC in this region is representative of the electron densities in the topside ionosphere and plasmasphere. Based on these observations alone it is not possible to distinguish between these two regions and we thus refer to these observations as the topside ionosphere-plasmasphere TEC throughout the remainder of the text. However, we should note that during 2008, the transition height from an O^+ dominated ionosphere to one dominated by light ions (H^+ and He^+) is near 800 km [*Tulasi Ram et al.*, 2010] The COSMIC POD TEC observations can thus be considered as primarily representative of the TEC in the plasmasphere. The TEC is obtained from the GPS observables of phase and pseudorange and details concerning the methods used to determine the TEC are given by *Pedatella and Larson* [2010] and not repeated herein. For the present study, all of the quiet time ($K_p < 3$) vertical TEC observations from the POD antennae during 2008 are binned in magnetic latitude, geographic longitude, local time and day of year. The bin sizes are 2.5° in magnetic latitude, 24° in geographic longitude and 2 h in local time. Note that in the analysis we mix magnetic and geographic coordinates since the longitude variations in the ionosphere are typically considered in a geographic coordinate frame. Magnetic latitude is used since the TEC is generally symmetric about the magnetic equator. The binning is performed using a running 45 day window of observations centered on each day of the year. The observations are fairly evenly distributed throughout the data bins and each bin has ~400–500 data points. Although the COSMIC provides adequate sampling on shorter time scales, a 45 day window of observations is used to reduce the effect of data noise, which may arise due to multipath, while still providing an adequate characterization of the seasonal variations.

2.2. Observations of TEC Below 800 km

[9] In order to study the longitude variations at predominately *F* region altitudes, COSMIC observations of vertical electron density profiles obtained through the technique of GPS radio occultation are used. The COSMIC electron density profiles extend up to ~800 km altitude and are in general agreement with incoherent scatter radar and ionosonde observations [*Lei et al.*, 2007; *Kelley et al.*, 2009]. For the present study, we use electron density profiles during quiet time periods ($K_p < 3$) of 2008 obtained through the COSMIC Data Analysis and Archive Center (CDAAC) (http://cosmic-io.cosmic.ucar.edu/cdaac/). For all profiles that extend upward of 750 km, the measured electron densities are used to calculate the integrated TEC between 250 km and top of the profile. Only profiles with a maximum altitude of greater than 750 km are used so that all of the computed TEC values encompass roughly the same altitude domain. Note that the upper boundary of the computed TEC is slightly variable. However, the upper boundary altitudes vary by ~50 km, and this is not thought to have any impact on the results. Although the altitude of the upper boundary is variable, throughout the remainder of the text, for ease of discussion, we refer to the upper boundary as being 800 km. The lower altitude of 250 km is selected to minimize errors that may be introduced by the Abel inversion used to obtain the electron density profile [e.g., *Liu et al.*, 2010]. Although we integrate up to ~800 km, the TEC in this altitude region will largely be dominated by electron densities in the *F* region and thus these observations are suitable for studying variations primarily occurring at *F* region altitudes. The COSMIC electron density profiles are not strictly vertical profiles and the computed TEC for each electron density profile is geographically located at the latitude and longitude of the tangent point corresponding to the maximum electron density. To facilitate comparison with the results for altitudes above the COSMIC satellite altitude, the TEC from the COSMIC electron density profiles are binned using the same method as discussed in section 2.1 for binning of the topside ionosphere-plasmasphere TEC. We do note, however, that there are considerably fewer data points for the COSMIC TEC below 800 km and each bin contains ~15–25 points. This difference is primarily driven by the different temporal sampling of GPS radio occultation compared the TEC observations from the POD antenna. While the POD data are nearly continuous, GPS radio occultation data are only available when the geometry between the COSMIC and a GPS satellite is suitable and

thus there are significantly fewer GPS radio occultation observations.

3. Model Description

[10] To investigate the source of the longitude variations in the *F* region ionosphere and the topside ionosphere and plasmasphere we have coupled the Global Ionosphere Plasmasphere (GIP) model [*Millward et al.*, 2007] to the National Center for Atmospheric Research (NCAR) Thermosphere Ionosphere Electrodynamics General Circulation Model (TIE-GCM) [*Richmond et al.*, 1992]. A brief description of the individual models is provided below along with details regarding the coupling of the two models.

[11] The GIP model is based on the ionosphere-plasmasphere part of the Coupled Thermosphere Ionosphere Plasmasphere (CTIP) model [*Millward et al.*, 2001] and solves the coupled equations of continuity, momentum and energy balance in a magnetic coordinate system. Densities, temperatures and velocities are calculated for O^+ and H^+ ions and the additional ions (N^+, N_2^+, O_2^+, NO^+) are calculated based on chemical equilibrium. In the GIP model, the equations are solved along realistic geomagnetic field lines based on the magnetic apex coordinate system [*Richmond*, 1995] and the International Geomagnetic Reference Field (IGRF). This represents a significant improvement upon the dipole geomagnetic field utilized in the CTIP model since the GIP includes distortions of the geomagnetic field which can have a significant influence on the ionosphere. The GIP model is separated into a low- to middle-latitude region where interhemispheric transport along flux tubes is taken into account and a high-latitude portion where there is no plasma flux across an upper boundary of 10000 km. For the present study we are only concerned with the low- to middle-latitude region which extends to $L = 4$ (~60° magnetic latitude), where L is the L shell [*McIlwain*, 1961]. The flux tubes in the low- to middle-latitude region are spaced 4.5° in magnetic longitude and each magnetic meridian includes 67 flux tubes in latitude (or altitude). The base of each magnetic flux tube is at 90 km and they extend to ~19000 km. Last, we note that the GIP only solves for the ions and electrons in the ionosphere and plasmasphere and does not include calculation of the thermosphere or electrodynamics. It thus requires input of the neutral thermosphere and $\mathbf{E} \times \mathbf{B}$ drift velocities from an external source, such as an empirical model.

[12] The TIE-GCM globally solves the dynamical equations for the thermosphere and ionosphere with self-consistent electrodynamics. The electrodynamics are calculated using a realistic geomagnetic field (IGRF) and magnetic apex coordinate system [*Richmond*, 1995]. At each time step the model calculates the neutral temperature, winds, and densities of various atmospheric constituents as well as the ionospheric structure on fixed pressure levels. The resultant neutral winds, ion densities, and calculated conductivities are then used to solve for the electric potential at each time step. For the present study, the TIE-GCM is run with a horizontal resolution of 2.5° in geographic latitude and longitude and a vertical resolution of four points per scale height. The lower boundary of the model is at approximately 97 km and the upper boundary ranges from 400 to 700 km depending on solar flux conditions.

[13] In an effort to improve upon the shortcomings in each model, we have coupled the GIP model to the TIE-GCM. Hereafter we will refer to the coupled model as GIP-TIEGCM. There are two significant advantages resulting from this coupling. First, the neutral thermosphere and electrodynamics that need to be specified for the GIP can be solved directly in a self-consistent manner and thus do not need to be based on empirical thermosphere or electrodynamic models. The coupling of these two models also eliminates the artificial upper boundary of the TIE-GCM. It is thus no longer necessary to specify ion number and electron heat fluxes between the ionosphere and plasmasphere across the model upper boundary. This should, in principal, improve the description of the low-latitude ionosphere and electrodynamics. Rather than including an interface between the two models at the upper boundary of the TIE-GCM, the models are completely coupled and the ionosphere in the TIE-GCM is entirely replaced by the GIP ionosphere. The TIE-GCM electrodynamics solver is used and the necessary field line integrals of conductivity and wind-driven current density are calculated along the GIP flux tubes. The electric fields calculated within the TIE-GCM are then used to calculate the vertical and zonal $\mathbf{E} \times \mathbf{B}$ drift velocities used for the ionospheric calculations. In the GIP model we have included zonal $\mathbf{E} \times \mathbf{B}$ drifts which represents an improvement upon the original CTIP model which only includes drift in the magnetic meridional plane. The inclusion of zonal drifts in the model is important for the present study since they may contribute to longitudinal variations in the topside ionosphere [e.g., *Huang et al.*, 2010]. The TIE-GCM also provides the neutral thermosphere densities, temperature, and winds that are required for the GIP calculations. The TIE-GCM electron temperature calculation is also used in the coupled model. Because neutral hydrogen is not included in the TIE-GCM, in the coupled model it is still specified empirically based on the Mass Spectrometer Incoherent Scatter (MSIS) model [*Picone et al.*, 2002]. Since the height domains of the GIP and TIE-GCM models are different, it is necessary to make some assumptions regarding the neutral thermosphere so that it encompasses the entire GIP grid. Above and below the TIE-GCM domain we assume constant winds and neutral temperatures. The individual constituents of the neutral atmosphere are extrapolated assuming a constant scale height where the scale height is determined at each latitude and longitude grid point from either the highest (for extrapolating up) or lowest (for extrapolating down) two grid points in the vertical direction. Because we use the electron temperatures calculated by the TIE-GCM, it is also necessary to extrapolate the electron temperatures to encompass the entire GIP domain. The extrapolation of electron temperatures is slightly more complex than the neutral thermosphere due to its height variation. Up to 350 km altitude, the electron temperatures are based on those calculated by the TIE-GCM. Above this altitude, the electron temperature is extrapolated along field lines based on the temperature and vertical gradient at 350 km. Details on the field line extrapolation of electron temperatures can be found in *Titheridge* [1998]. Note that the coupled GIP-TIEGCM is still in a developmental stage; however, for the purposes of the present study, it has been adequately tested to confirm that the model provides reasonable results.

[14] The GIP-TIEGCM has been used to perform several simulations in an effort to reproduce and understand the causes of observed longitude variations in both the *F* region as well as the topside ionosphere and plasmasphere. Simulations have been performed for September equinox and December solstice under solar quiet (F10.7 = 60 $10^{-22} Wm^{-2}\ Hz^{-1}$) conditions. Note that the mean solar flux during 2008 was 69 $10^{-22} Wm^{-2}\ Hz^{-1}$, and thus this solar flux is slightly below the actual conditions during 2008. However, it was necessary to run the model at a slightly lower solar flux so that the *F* region electron densities from the model match observations during 2008. Each simulation is initialized from a 20 day run of TIE-GCM (version 1.92). The coupled model is then run for 10 days so that the model reaches a steady state. Two simulations are performed for each season: one where the TIE-GCM lower boundary near 97 km is forced with diurnal and semidiurnal migrating and nonmigrating tides and another with no tidal forcing at the lower boundary. This allows us to separate the effects of longitude variations due to nonmigrating tides and those that may be related to the orientation of the geomagnetic field. The lower boundary tidal forcing is based on Hough Mode Extensions (HMEs) obtained from Thermosphere Ionosphere Mesosphere Energetics and Dynamics (TIMED) TIMED Doppler Interferometer (TIDI) and Sounding of the Atmosphere using Broadband Emission Radiometry (SABER) observations [*Forbes et al.*, 2009; *Oberheide et al.*, 2009, 2011]. The HMEs used are based on observations from 2002 to 2008 and thus are considered to be representative of the tidal climatology at ~97 km. In September, as shown in the following section, the daytime ionosphere exhibits a distinct wave 4 pattern and prior studies have connected this longitude variation to the *DE*3 tide [e.g., *Immel et al.*, 2006; *Wan et al.*, 2008]. We have adjusted the *DE*3 amplitude and phase at the lower boundary during September in order to achieve good agreement between the observations and model results for the TEC up to 800 km. As the present study is primarily concerned with the difference in longitude variations of TEC above and below 800 km we have chosen to adjust the model forcing so that the model results above 800 km should be representative of the actual conditions. Adjusting the model forcing in this manner permits a more accurate comparison with observations of the topside ionosphere-plasmasphere TEC. A mixture of nonmigrating tides is likely to create the longitude variations that are observed in December and this complicates any adjustment of the lower boundary forcing to match the observations as was done for the September simulations. We therefore do not make any effort to adjust the lower boundary forcing for the December simulation.

[15] For comparison with the observations, the model results are used to calculate the TEC in the topside ionosphere-plasmasphere up to 20200 km. Since the model domain extends only to ~19000 km at the magnetic equator, and less at higher latitudes, we extrapolate the electron densities up to 20200 km. The extrapolation is done by first mapping the electron densities along the flux tube grid onto a fixed latitude, longitude, and altitude grid. The grid spacing is 3° in magnetic latitude, 4° in geographic longitude, and in the vertical ranges from 5 km at low altitudes to 500 km at high altitudes. The electron density at each grid point is calculated based on a distance weighted average of the electron densities at flux tube points that are within the grid point domain (i.e., within ±1.5° latitude, ±2° longitude and variable height depending on the altitude). For each latitude and longitude the electron density is then extrapolated in the vertical direction up to 20200 km based on a constant scale height which is determined from the two highest grid points that are within the $L = 4$ outer boundary of the flux tubes. At higher latitudes, this can result in extrapolating over large altitude regions. The present study is, however, primarily focused on low latitudes where any errors associated with the height extrapolation of electron densities should be minimal.

4. Results

[16] The longitudinal variations averaged between 1600 and 1800 local time (LT) of the TEC at altitudes above and below 800 km that are observed by the COSMIC satellites and simulated by the GIP-TIEGCM are presented in Figures 1 and 2 for September equinox and December solstice, respectively. The results for 1600–1800 LT can be considered as generally representative of the longitude variations during the daytime and this fact will be shown in Figures 3 and 4. As expected, around September equinox, the longitude variations in the *F* region ionosphere (Figures 1a and 1c) exhibit a primarily wave 4 structure which is attributed to forcing by the *DE*3 tide. A similar wave 4 feature in longitude is also apparent in both the observations and model results of the topside ionosphere-plasmasphere as shown in Figures 1b and 1d. In both of these altitude regions, the GIP-TIEGCM is generally able to reproduce the COSMIC observations. In the *F* region, the modeled longitude variations of the maxima in the EIA crest region match the regions of enhanced density observed by the COSMIC. This correspondence is to be expected since we have adjusted the amplitude and phase of the *DE*3 forcing at the model lower boundary to obtain an agreement with the observations. Although the longitude variations are in good agreement, the GIP-TIEGCM results show a more distinct EIA compared to the observations. Depending on the geometry of the COSMIC-GPS raypath, there can be a difference of several degrees in latitude and longitude between the top and bottom of the COSMIC electron density profiles and this has the potential to smooth the EIA in the observations. The lack of distinct EIA in the observations may also be related to the assumption of spherical symmetry when determining the electron densities using GPS radio occultation. This assumption can introduce significant errors in the equatorial anomaly region [*Yue et al.*, 2010]. In the topside ionosphere-plasmasphere TEC, although both the model and observations reveal a wave 4 structure in longitude, there is some discrepancy in the location of the maxima. Both the model and observations have maxima near 100° and 200° geographic longitude but the locations of the other two maxima are slightly different. It is also clear that while the model and observations reveal similar longitude variations in the topside ionosphere-plasmasphere, they differ considerably in absolute terms and the observations tend to be 2–3 TECu (1 TECu = 10^{16} el/m^2) (~20% at the maxima in longitude) larger. It is not known why the model and observations differ by a few TECu in absolute terms. However, in the present study we are

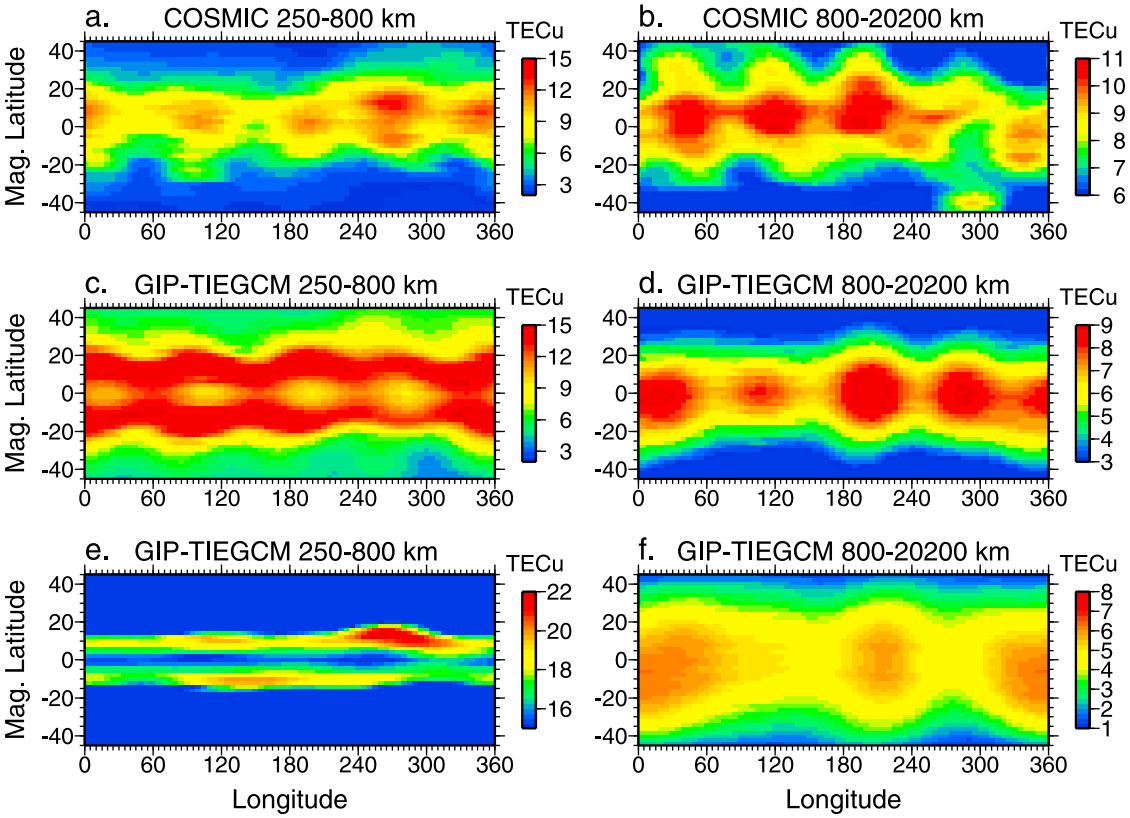

Figure 1. Geographic longitude and magnetic latitude variations of the TEC between 1600 and 1800 LT around September equinox for (a) COSMIC observations below 800 km, (b) COSMIC observations above 800 km, (c) GIP-TIEGCM simulation below 800 km with tidal forcing, (d) GIP-TIEGCM simulation above 800 km with tidal forcing, (e) GIP-TIEGCM simulation below 800 km without tidal forcing, and (f) GIP-TIEGCM simulation above 800 km without tidal forcing.

interested in the relative longitudinal variations, which are well reproduced by the model, and thus the slight difference in absolute TEC is inconsequential.

[17] The model results without tidal forcing are shown in Figures 1e and 1f and longitude variations are apparent. Similar to *Hagan et al.* [2007], in the absence of nonmigrating tides, only small longitudinal variations occur in the *F* region ionosphere. The situation in the topside ionosphere-plasmasphere TEC is different and even without tidal forcing significant longitude variations are present (Figure 1f). However, comparison of Figure 1c with Figure 1e and Figure 1d with Figure 1f reveal that the longitude variations without tidal forcing are significantly different than those that occur in the presence of tidal forcing. This clearly demonstrates that including nonmigrating tidal forcing in the model is important for reproducing the observed longitude variations. The generation of longitude variations in the absence of tidal forcing will be discussed in detail later.

[18] The observations and model results for December solstice (Figure 2) again reveal considerable longitude variations in the *F* region ionosphere as well as the topside ionosphere-plasmasphere. These variations are, however, considerably different than those that occur around September equinox due to the dominance of different nonmigrating tides during this time period [*Forbes et al.*, 2008]. The observations exhibit notable maxima in the *F* region between roughly 70°–120° and 300°–360°. This longitude variation may be related to the tidal forcing being dominated by *DE*2 and *SW*4 during Northern Hemisphere winter [*Forbes et al.*, 2008; *Pedatella et al.*, 2008]. The model results in the *F* region also exhibit enhancements around 60°–120° and 300°–360°; however, a maximum is also observed around 200°–260° geographic longitude. The difference in the observed and modeled longitude variation may be related to the climatological forcing that is used at the model lower boundary which may not be fully representative of the conditions during December 2008. The difference could also be related to inaccurate vertical propagation of the tides in the model during December solstice. In the topside ionosphere-plasmasphere, both the model and observations reveal a significant maximum in the TEC beginning around 260° longitude and this feature extends beyond 0° longitude. There are also smaller secondary maxima near 120° and 200° longitude in the observation results. While there is some indication of an enhancement around 120° geographic longitude in the model simulation with tidal forcing, the observed secondary maxima are largely absent from the model results. We again note that significant longitude variations exist in the absence of tidal forcing as can be seen in Figures 2e and 2f. Contrary to the September simulation results, the GIP-TIEGCM simulations with and without tidal forcing for December solstice reveal similar longitude variations in the topside ionosphere-

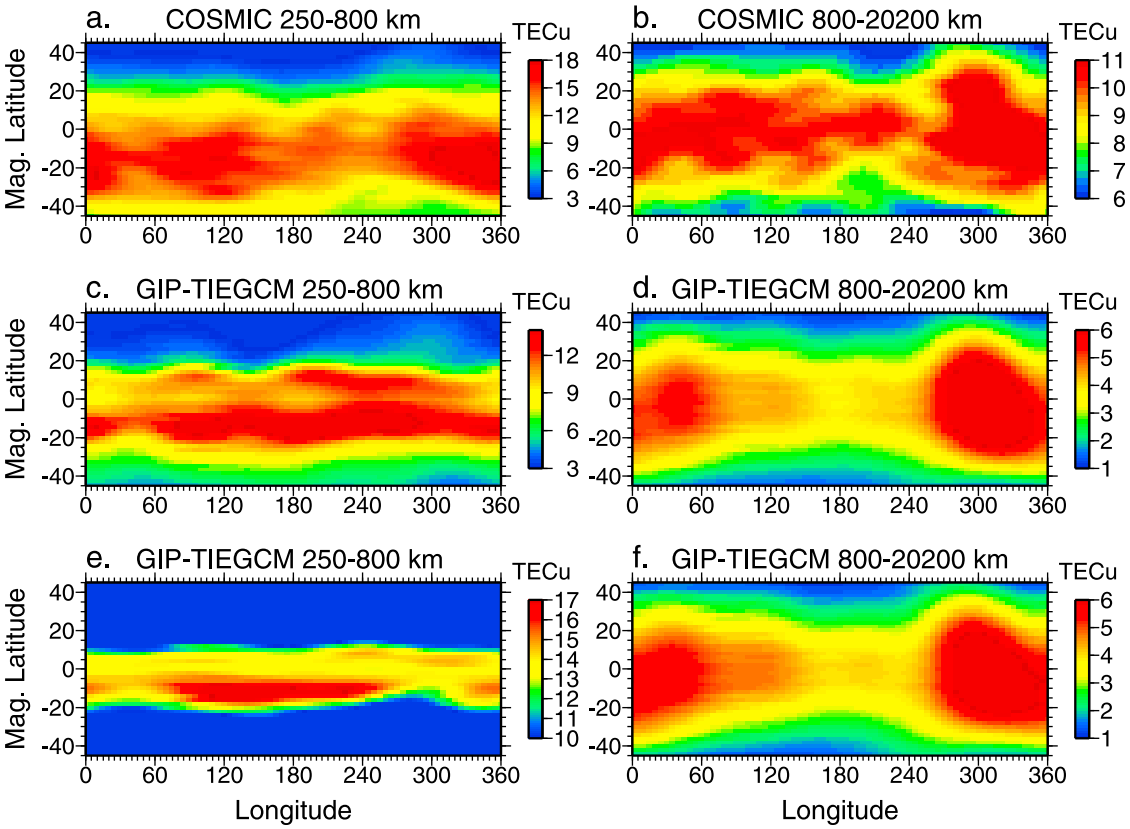

Figure 2. Same as Figure 1 except for December solstice conditions.

plasmasphere TEC. This indicates that the primary longitude variation present in the topside ionosphere-plasmasphere TEC near December solstice is not the result of nonmigrating tides. We will discuss the formation mechanism of this feature in detail later.

[19] The evolution of the longitude variations with local time for September equinox and December solstice are presented in Figures 3 and 4, respectively. The results presented in Figures 3 and 4 correspond to the average TEC between 10°N and 20°N magnetic latitude for the region below 800 km and between ±10° magnetic latitude for the topside ionosphere-plasmasphere. These latitudes correspond to the regions where the longitude variations are most pronounced. During the daytime, Figures 3 and 4 reveal similar longitude variations as shown in Figures 1 and 2. In December, it is worth noting that both the observations (Figure 4a) and model results (Figure 4c) of the *F* region show fairly similar longitude variations during the daytime. However, there is a slight shift in the local time of the longitude variations and this may account for some of the disagreement between the longitude variations shown in Figures 2a and 2c. There is a clear difference in the local time behavior of the longitude variations in the two altitude regions. In the *F* region, a similar longitude structure tends to dominate at all local times. For example, around September equinox both the observations (Figure 3a) and GIP-TIEGCM simulation (Figure 3c) reveal a primarily wave 4 feature at all local times. Presuming that the *DE*3 is the only tide responsible for generating the wave 4 feature in the *F* region, a phase shift of 90°/24 h LT should occur. The dashed lines in Figures 3a and 3c indicate this phase shift. Although there is a phase shift in the observed and modeled wave 4 feature in the *F* region, it is not exactly 90°/24 h LT. This indicates that other nonmigrating tides may be contributing to the wave 4 variation as suggested by *Oberheide et al.* [2011]. The slightly different phase shift may also be related to zonal $\mathbf{E} \times \mathbf{B}$ drifts which may decrease the phase shift during the day and increase the phase shift at night [*Wan et al.*, 2008]. The fact that the longitude variation in the ionosphere at a given local time represents the instantaneous tidal response combined with the longitude variations from earlier local times may also contribute to the different phase shift. Unlike the *F* region, in the topside ionosphere-plasmasphere significant differences are observed in the daytime and nighttime longitude variations. This is particularly apparent around September equinox where the wave 4 structure that is present during the daytime is no longer apparent at night. At night, there tends to be two regions of enhanced TEC in the topside ionosphere-plasmasphere TEC. Although to a lesser extent, different longitude variations can also be observed in the daytime and nighttime topside ionosphere-plasmasphere TEC during December solstice.

[20] The seasonal change of the longitude variations observed by the COSMIC satellites in the *F* region and topside ionosphere-plasmasphere TEC are presented in Figures 5a and 5b, respectively. The results shown in Figure 5 are the average TEC between 1200 and 1800 local time for the same latitude ranges used in Figures 3 and 4. Figure 5a reveals the emergence of a wave 4 variation in longitude during Northern Hemisphere summer that

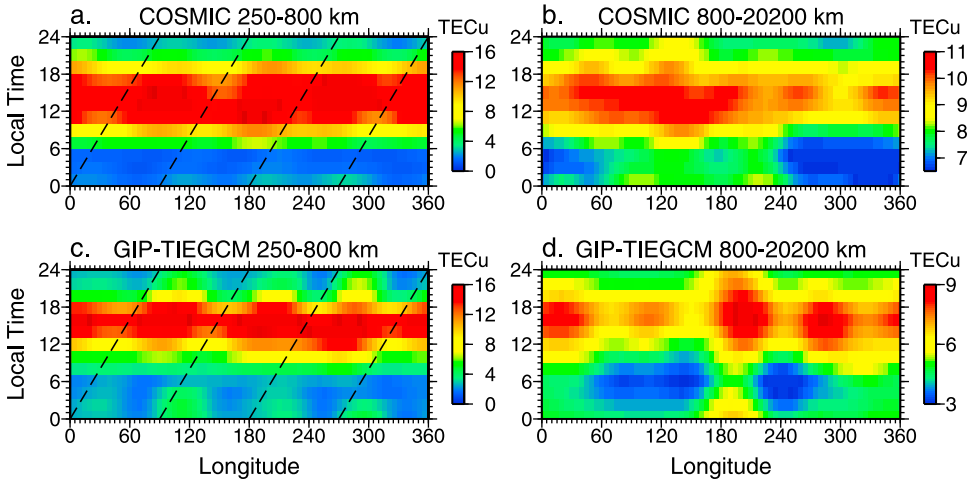

Figure 3. The local time and longitude variation of the TEC around September equinox for (a) COSMIC observations below 800 km, (b) COSMIC observations above 800 km, (c) GIP-TIEGCM simulation below 800 km, and (d) GIP-TIEGCM simulation above 800 km. The results for the TEC below 800 km are averages between 10 and 20°N magnetic latitude, and the TEC above 800 km are averaged between ±10° magnetic latitude. The dashed lines in Figures 3a and 3c indicate a phase shift of 90°/24 h LT which is the expected phase speed of the *DE*3 in a fixed local time frame.

extends into October (day of year 275–305). In Northern Hemisphere winter three maxima (or minima) are apparent. During this time period, minima can be observed near 60°, 170°, and 340° geographic longitude. The presence of three maxima (or minima) in longitude during Northern Hemisphere winter is consistent with prior observations in the *F* region [*Pedatella et al.*, 2008; *Scherliess et al.*, 2008]. In the topside ionosphere-plasmasphere TEC (Figure 5b), perhaps the most striking feature is the large seasonal variation that occurs between 300° and 360° geographic longitude. The topside ionosphere-plasmasphere TEC is significantly enhanced in this region during Northern Hemisphere winter and exhibits a large depletion during Northern Hemisphere summer. A similar feature and seasonal variation has previously been observed in the both the topside ionosphere and plasmasphere. *Clilverd et al.* [1991] presented observations and model results indicating that at $L = 2.5$ a large seasonal variation exists near 300° geographic longitude, but is absent at other longitudes. This same seasonal variation near 300° geographic latitude has also been observed at dusk in the ion density at 840 km [*Huang et al.*, 2010], and in topside ionosphere electron densities near 600 km [*Kakinami et al.*, 2011]. Other longitude variations are also present and, similar to the *F* region, a wave 4 variation is observed around both March (day of year 80) and September (day of year 265) equinoxes.

5. Discussion

[21] Figures 1–5 clearly demonstrate the presence of longitude variations in both the *F* region ionosphere and

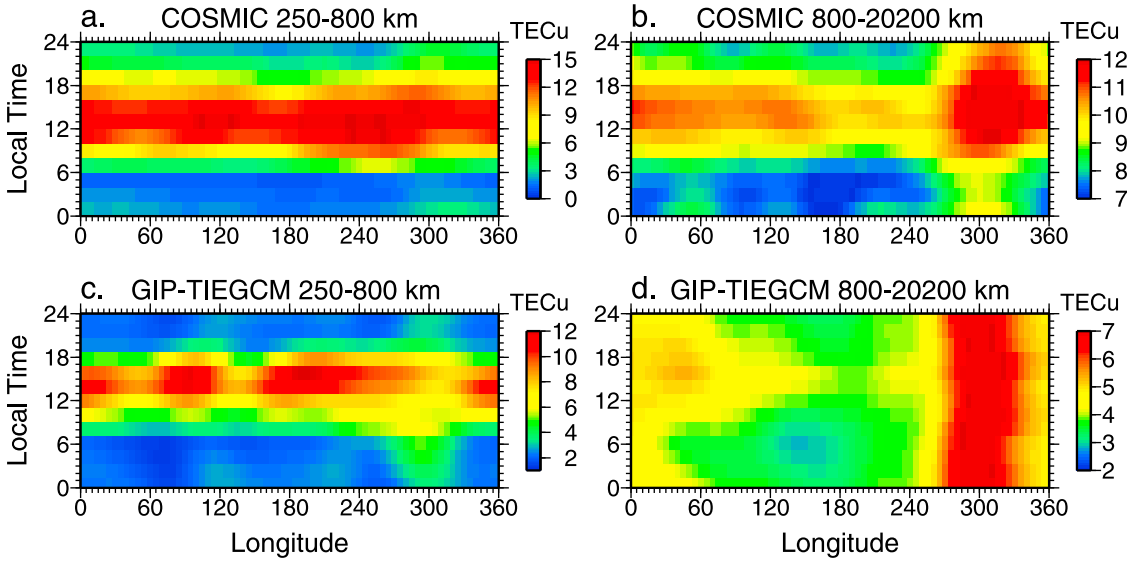

Figure 4. Same as Figure 3 except for December solstice conditions.

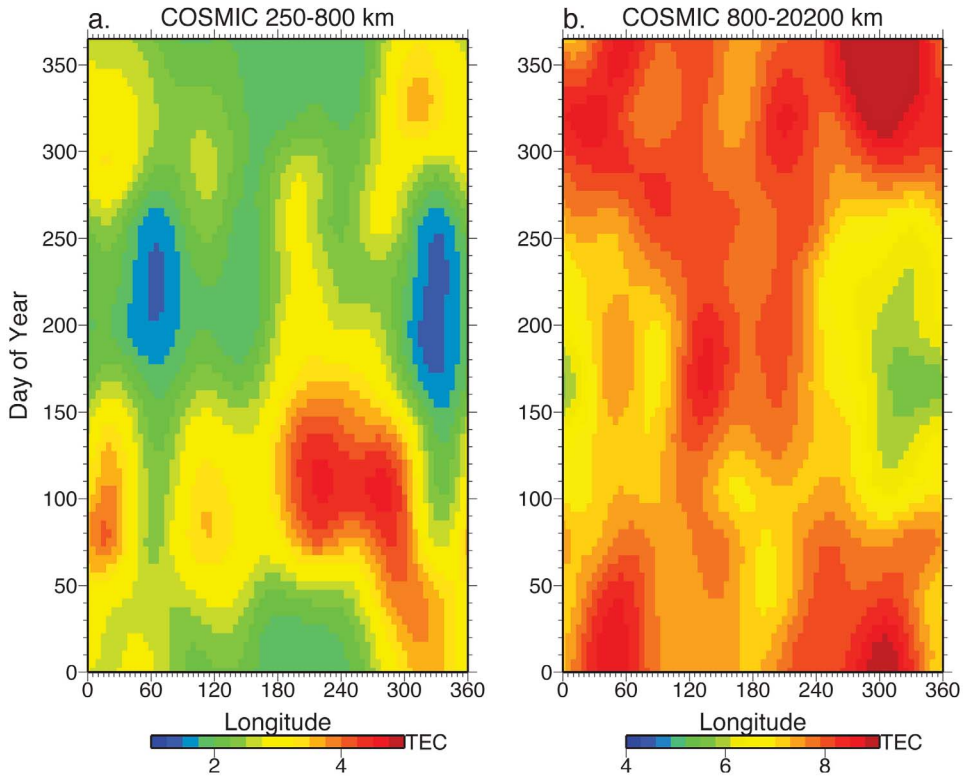

Figure 5. The seasonal variation of the longitude structures observed by COSMIC (a) below 800 km and (b) above 800 km. The TEC is averaged between 1200 and 1800 local time and 10 and 20°N magnetic latitude for the observations below 800 km and ±10° for above 800 km.

topside ionosphere-plasmasphere TEC. There are also considerable seasonal and local time variations as previously mentioned. We now turn our attention to understanding the causes of the observed and modeled longitude variations in the topside ionosphere-plasmasphere as well as their similarities and differences with those in the *F* region. By far the most dominant feature in the topside ionosphere-plasmasphere is the significant seasonal variation observed in the TEC between 300° and 360° geographic longitude. Furthermore, this feature is not apparent in the *F* region indicating that the mechanism by which this feature is generated is altitude dependent. As previously mentioned, *Huang et al.* [2010] observed a similar feature and seasonal variation in the topside ionosphere ion densities at dusk near 840 km and they attributed this feature to the large declination of the geomagnetic field in this longitude sector. The combination of the geomagnetic field declination along with the seasonal variation in the neutral winds is thought to either enhance or reduce the field-aligned component of the neutral wind. This results in the large topside ionosphere ion densities (or TEC) during Northern Hemisphere winter and a depletion during Northern Hemisphere summer [*Huang et al.*, 2010]. The field-aligned wind component can significantly influence densities in the topside ionosphere [e.g., *Watanabe and Oyama*, 1996; *Kil et al.*, 2006] and this effect is therefore most pronounced in the topside ionosphere-plasmasphere in spite of its absence in the *F* region. *Hartman and Heelis* [2007] observed a similar longitude and seasonal variation in the topside ionosphere vertical $\mathbf{E} \times \mathbf{B}$ drifts at dawn. They attributed the longitudinal variations observed near the solstices to be due to the relative orientation of the terminator and magnetic meridian in regions of large declination. While this may explain the longitude variations at dawn, in regions of large declination, Figure 4 demonstrates that the enhancement in the topside ionosphere-plasmasphere TEC is observed at all local times. The fact that this feature is present at all local times tends to support the hypothesis that it is generated by enhanced field-aligned winds associated with the orientation of the geomagnetic field.

[22] To understand how the geomagnetic field orientation can introduce the significant seasonal variation around 300°–360° longitude, we have also performed a GIP-TIEGCM simulation without tidal forcing for June solstice. The topside ionosphere-plasmasphere TEC from the GIP-TIEGCM simulations without tidal forcing for June and December solstice near the magnetic equator are shown as a function of local time and longitude in Figures 6a and 6b, respectively. Similar to the observations, the topside ionosphere plasmasphere TEC near 300° longitude is enhanced during December solstice and decreased during June solstice, and this is true for all local times. The model results for June solstice also reveal an enhancement around 180° longitude. Although not as strong as in the GIP-TIEGCM simulation, a similar enhancement is observed in the COSMIC topside ionosphere-plasmasphere TEC (Figure 5b). Variations at longitudes near 300° have previously been attributed to the influence of neutral winds [*Watanabe and Oyama*, 1996; *Ren et al.*, 2008; *Huang et al.*, 2010]. To investigate the role of neutral winds in

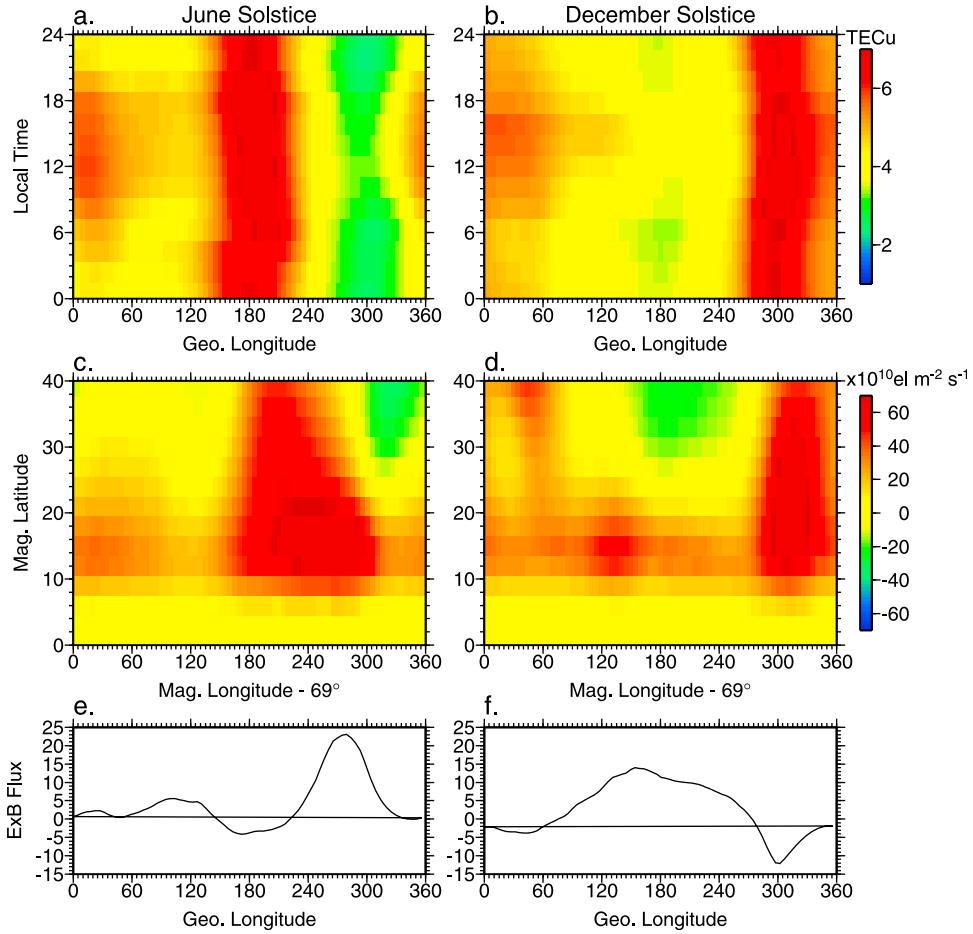

Figure 6. GIP-TIEGCM simulation without tidal forcing. (a) Local time and longitude variation of TEC above 800 km averaged between ±10° magnetic latitude for June solstice. (b) Same as Figure 6a except for December solstice. (c) North-south average of the daily average vertical wind driven flux at 500 km for June solstice. (d) Same as Figure 6c except for December solstice. (e) Daily average **E** × **B** flux at 800 km at the magnetic equator for June solstice. (f) Same as Figure 6e except for December solstice. The units of the **E** × **B** flux are $10^{10} elm^{-2}\, s^{-1}$. Note that Figures 6a, 6b, 6e, and 6f are in are in geographic longitude, while Figures 6c and 6d are in magnetic longitude shifted by 69°. The reason for using magnetic longitude in Figures 6c and 6d is explained in the text.

establishing this longitudinal variability, Figures 6c and 6d show the north-south daily average vertical component of the field-aligned wind driven flux at 500 km. This is given by

$$\frac{\left(\frac{U_{||,s}N_{e,s}\sin(I_s)}{B_{r,s}} - \frac{U_{||,n}N_{e,n}\sin(I_n)}{B_{r,n}}\right)}{2}\frac{\left(B_{r,s} - B_{r,n}\right)}{2} \qquad (1)$$

where $U_{||}$ is the field-aligned neutral wind, N_e is the electron density, I is the inclination angle, and B_r represents the radial component of the geomagnetic field. The subscripts n and s in equation (1) indicate values at 500 km in the Northern and Southern Hemispheres, respectively. Note that in equation (1), the $U_{||}N_e\sin(I)$ term represents the vertical plasma drift due to neutral wind. Since the filling of a plasma flux tube depends on the flux tube area, which is inversely proportional to the magnetic field strength, this term is divided by the radial magnetic field strength. Further note that we weight the north-south average by the radial magnetic field strength, and this results in inclusion of the final term in equation (1). We calculate the vertical component of the field-aligned wind driven flux based on equation (1) for each flux tube so that the values at 500 km in the Northern and Southern Hemispheres are magnetically conjugate points. We thus present results in Figures 6c and 6d in terms of magnetic longitude; however, for ease of comparison with our prior results, we have shifted the magnetic longitude so that the shifted magnetic longitude corresponds roughly to geographic longitude. Note that the results in Figures 6c and 6d are for an altitude of 500 km since we presume that the neutral wind driven plasma that generates the longitude variations in the TEC at the magnetic equator above 800 km originates at lower altitudes in the low- to middle-latitude region. Further, we present the daily average flux since, presuming that the longitude variations in the topside ionosphere-plasmasphere TEC are driven primarily by neutral wind effects, longitudes with a larger daily average vertical wind driven flux are expected

be related to enhancements in the topside ionosphere-plasmasphere TEC. Comparison of the daily average vertical component of the field-aligned flux with the topside ionosphere-plasmasphere TEC reveals that the longitudes of enhanced TEC correspond to greater vertical fluxes at low to middle latitudes. The regions of enhanced TEC could also be related to the vertical $\mathbf{E} \times \mathbf{B}$ flux. The daily average vertical $\mathbf{E} \times \mathbf{B}$ fluxes at 800 km at the magnetic equator for June and December solstices are shown in Figures 6e and 6f. The vertical $\mathbf{E} \times \mathbf{B}$ flux is given by $N_e V_{ExB,vert}$ where $V_{ExB,vert}$ is the vertical component of the $\frac{ExB}{B^2}$ velocity. Note that the $\mathbf{E} \times \mathbf{B}$ fluxes are for 800 km (opposed to 500 km for the wind driven flux) since we are interested in the vertical flux at this altitude for comparison with the topside ionosphere-plasmasphere TEC. There does not appear to be a strong connection between the longitude variations in vertical $\mathbf{E} \times \mathbf{B}$ flux and the topside ionosphere-plasmasphere TEC. In fact, near 300° geographic longitude, the daily average vertical $\mathbf{E} \times \mathbf{B}$ flux tends to be anti-correlated with the topside ionosphere-plasmasphere TEC. This indicates that the significant longitude variations that occur near solstice in the topside ionosphere-plasmasphere TEC are the result of field-aligned winds which can either enhance or suppress the vertical transport. The variations in the field-aligned winds are a combination of two effects. First, in regions of large magnetic declination, the zonal winds produce a significant field-aligned component. The meridional winds also contribute due to the offset between the geographic and geomagnetic equators. The fluxes in Figures 6c and 6d represent a combination of the meridional and zonal wind effects. The fluxes may also be influenced by hemispheric asymmetry of the electron density.

[23] The effect of the geomagnetic field alone appears to generally have a greater influence on producing longitude variations in the topside ionosphere-plasmasphere than in the *F* region. Nonetheless, the geomagnetic field does introduce some longitude variability in the *F* region as can be observed in Figures 1e and 2e. The GIP-TIEGCM simulations reveal a considerable seasonal variation of the relative importance of nonmigrating tides and the geomagnetic field for producing the longitude variations. Comparison of Figures 1c and 1e demonstrate that, for September equinox, the inclusion of nonmigrating tides drastically changes the longitude variations at 1600–1800 LT in the *F* region ionosphere. The situation in December (Figure 2) is rather different, and there is some degree of similarity between the GIP-TIEGCM simulations with and without tidal forcing. For example, the simulations both with and without tidal forcing reveal enhancements in the *F* region TEC near ~100°, ~230°, and ~350° longitude. These results indicate that during time periods around September equinox, when the amplitude of *DE*3 is large, the ionospheric longitude variations are dominated by the nonmigrating tides while during Northern Hemisphere winter the role of nonmigrating tides may be of lesser (although not insignificant) importance. That is, during Northern Hemisphere winter, nonmigrating tides and the geomagnetic field orientation may be of roughly equal importance whereas around September equinox the role of nonmigrating tides appears to be of significantly more importance than the geomagnetic field.

[24] While the geomagnetic field clearly plays a significant role in producing longitude variations in the topside ionosphere-plasmasphere, both the COSMIC observations and GIP-TIEGCM simulations reveal the presence of additional features which are not explained by the geomagnetic field alone. This fact is especially apparent around September equinox when a notable wave 4 feature is observed in the topside ionosphere-plasmasphere TEC (Figures 1 and 3). As seen in Figure 1f, the geomagnetic field alone may introduce a wave 2 structure in longitude but both the observations (Figure 1b) and GIP-TIEGCM simulations with complete tidal forcing (Figure 1d) indicate a wave 4 structure in longitude. Similar to the numerous prior studies on longitude variations in the *F* region [e.g., *Immel et al.*, 2006; *Lin et al.*, 2007; *Wan et al.*, 2008] we consider this longitude structure in the topside ionosphere-plasmasphere TEC to be a signature of nonmigrating tidal influences. We consider several mechanisms which may produce the longitude variations in the topside ionosphere-plasmasphere TEC. First, observations reveal wave 4 longitude variations in the vertical $\mathbf{E} \times \mathbf{B}$ drifts at 840 km altitude [*Hartman and Heelis*, 2007; *Huang et al.*, 2010]. The longitude variations in the topside ionosphere vertical drifts can introduce similar variations in the topside ionosphere-plasmasphere TEC through vertical transport. Alternatively, nonmigrating tides may introduce longitudinal variability into the topside ionosphere-plasmasphere through tidally driven temperature variations which may modulate the topside ionospheric scale height. Evidence now exists that nonmigrating tides can penetrate into the thermosphere and influence thermospheric neutral densities and winds, as well as exospheric temperatures [*Forbes et al.*, 2009; *Talaat and Lieberman*, 2010]. In particular, the *DE*3 has been shown to directly penetrate into the thermosphere and exosphere [*Forbes et al.*, 2009; *Oberheide et al.*, 2009, 2011]. The direct penetration of *DE*3 to altitudes in excess of 800 km may play a critical role for introducing longitude variations in the topside ionosphere-plasmasphere TEC. Tidal variations in the topside ionosphere plasma temperature will introduce longitude variations in the topside ionospheric scale height, and thus influence the vertical distribution of plasma in the topside ionosphere-plasmasphere. We note that although previous studies [*Forbes et al.*, 2009; *Talaat and Lieberman*, 2010] have presented observational evidence for the penetration of *DE*3 into the thermosphere and exosphere, these studies have focused on neutral temperature variations, as opposed to plasma temperatures which are relevant for controlling the topside ionosphere scale height. However, associated with the neutral temperature variations are similar variations in density and neutral winds [e.g., *Oberheide et al.*, 2011]. These may influence the temperature and density in the topside ionosphere, and, in turn the topside ionosphere scale height [*Luan et al.*, 2006]. Furthermore, in the equatorial region, observations have revealed the presence of longitude variations in the topside ionosphere scale height [*Liu et al.*, 2008, 2011]. As discussed by *Liu et al.* [2011] these are considered to be connected to nonmigrating tides, and may be driven by either variations in temperatures or vertical $\mathbf{E} \times \mathbf{B}$ drifts.

[25] To investigate the cause of the longitude variations in the topside ionosphere-plasmasphere TEC during September equinox, Figures 7a and 7b present the local

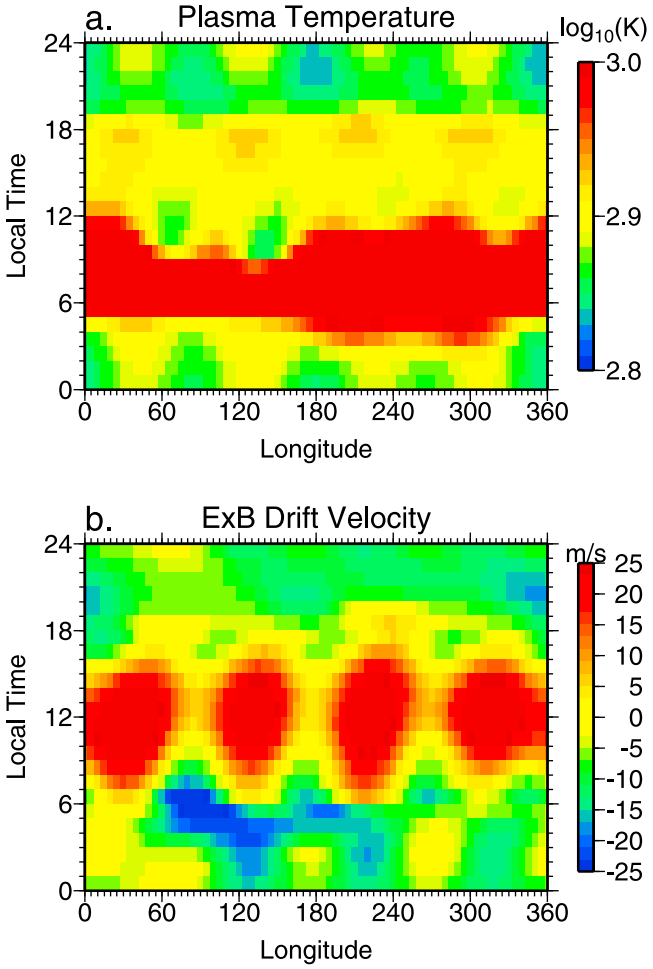

Figure 7. (a) Local time and longitude variation of the plasma temperature at the geomagnetic equator at 800 km. (b) Local time and longitude variation of the vertical **E** × **B** drift velocity at the geomagnetic equator at 800 km. The results are for the September equinox GIP-TIEGCM simulation with tidal forcing.

time and longitude variations of the plasma temperature and vertical **E** × **B** drift velocity, respectively. The results shown in Figure 7 are for the GIP-TIEGCM simulation for September equinox with tidal forcing, and are for an altitude of 800 km above the geomagnetic equator. Clear wave 4 longitude variations are apparent in both the plasma temperatures and **E** × **B** drift velocities. In the afternoon, when the wave 4 longitude variation in the topside ionosphere-plasmasphere is most prevalent, the regions of enhanced plasma temperatures appear to correspond to regions of enhanced TEC. Thus, the enhancements in TEC may be driven in part by temperature driven changes in topside ionosphere scale height. However, there are also clear wave 4 variations in the daytime vertical **E** × **B** drifts which may also contribute to the longitude variations in the topside ionosphere-plasmasphere TEC. The vertical drifts can introduce longitude variations in the topside ionosphere-plasmasphere TEC through both vertical transport and by influencing the scale height. The longitude variations in vertical scale height observed by *Liu et al.* [2011] may thus be due to a combination of temperature and vertical drift variations. Based on the above, we consider the topside ionosphere-plasmasphere TEC longitude variations to be driven by a combination of scale height variations and variations in vertical transport due to **E** × **B** vertical drifts. Unfortunately, it is difficult to separate the relative contribution of these two effects; however, our results suggest that both may contribute to a portion of the longitude variability.

[26] Nonmigrating tides may also influence the topside ionosphere-plasmasphere due to modulation of *F* region densities in combination with the diurnal exchange of plasma between the ionosphere and plasmasphere. In general, the flow between the ionosphere and plasmasphere is upward (flowing from the ionosphere to the plasmasphere) during the daytime and downward (flowing from the plasmasphere to the ionosphere) at night [*Schunk and Nagy*, 2000]. During the daytime, the vertical flow of plasma in longitude sectors of enhanced density in the *F* region may result in larger topside ionosphere-plasmasphere densities at these longitudes as well. The significant difference in the longitude variations in the topside ionosphere-plasmasphere during the daytime and nighttime supports the fact that these variations may, in part, originate in the *F* region. If the longitude variations in the topside ionosphere-plasmasphere partly result from the vertical flow of plasma from the *F* region then it is logical that they would disappear at night when plasma flows downward from the plasmasphere into the ionosphere. In fact, this downward flow could potentially serve to maintain the longitude variations in the nighttime *F* region.

[27] We consider all of the aforementioned mechanisms for nonmigrating tides generating longitude variations in the topside ionosphere-plasmasphere TEC to be plausible. The most likely scenario is that the longitude variations that are present in the topside ionosphere-plasmasphere TEC are due to a combination of **E** × **B** drifts, scale height variations, and vertical flow from the *F* region. It is difficult to specify the relative importance of each of these mechanisms. As mentioned previously, the geomagnetic field orientation also generates longitude variations. The actual longitude variations that are present will represent the effects due to nonmigrating tides combined with those due to the geomagnetic field.

6. Conclusions

[28] In the present study we have presented observations and model results of the seasonal and local time variability of longitude structures in the ionospheric TEC above and below 800 km altitude. This has revealed some of the similarities and differences of the longitude variations present in these two altitude regions. The COSMIC observations and GIP-TIEGCM simulations reveal the expected seasonal, local time, and latitude behavior of the longitude structures in the *F* region ionosphere. The results presented do, however, provide new insight into the longitude variations present in the topside ionosphere-plasmasphere. The most dominant feature in the topside ionosphere-plasmasphere TEC is a pronounced longitude and seasonal variation observed near 300°–360° geographic longitude. At all local times, this longitude region exhibits a distinct minimum during Northern Hemisphere summer while a maximum is

present during Northern Hemisphere winter. Results from a new coupled model indicate that this feature is not related to nonmigrating tides and it is thought to be due to the seasonal variation of the neutral winds generated in the thermosphere in combination with the geomagnetic field orientation.

[29] Both the COSMIC observations and GIP-TIEGCM results also reveal longitude variability in the topside ionosphere-plasmasphere TEC related to nonmigrating tides. This is most apparent in the distinct wave 4 variation in longitude that is present around September equinox in the daytime topside ionosphere-plasmasphere TEC. The GIP-TIEGCM simulations are able to reproduce this feature when nonmigrating tides are included at the lower boundary and thus indicate that the source of the longitude variations in the topside ionosphere-plasmasphere is nonmigrating tides. We attribute the existence of nonmigrating tidal variations at altitudes in excess of 800 km to several potential mechanisms. First, these may be connected to variations in the topside ionosphere scale height. The scale height variations are considered to be driven by some combination of vertical $\mathbf{E} \times \mathbf{B}$ drifts and variations in the plasma temperature. The longitude variations in the vertical $\mathbf{E} \times \mathbf{B}$ drift velocity may also drive the longitude variations in the topside ionosphere-plasmasphere TEC through influencing the vertical transport. Last, the nonmigrating tidal perturbations in the topside ionosphere-plasmasphere may be related to the upward flow of plasma from regions of enhanced density in the *F* region during the daytime. This second mechanism may explain the similarity between the *F* region and topside ionosphere-plasmasphere longitude structures during the daytime and the notable difference in the longitude variations at night when the direction of plasma flow is reversed. Ultimately the longitude variations present in the topside ionosphere-plasmasphere TEC are likely a mixture of effects due to nonmigrating tides as well as those due to the neutral winds in combination with the geomagnetic field orientation.

[30] **Acknowledgments.** We thank two anonymous reviewers for their helpful comments. Jens Oberheide is acknowledged for providing the climatological HMEs used in the present study. The authors wish to thank the COSMIC Data Analysis and Archive Center for making available the COSMIC observations used in the present study. This work was supported by a National Science Foundation Graduate Research Fellowship (N. Pedatella) and by grant NNX08AF22G from the NASA Guest Investigator Program to the University of Colorado. A. Maute, A. D. Richmond, and T.-W. Fang were partly supported by NSF award ATM-0836386 and NASA grant NNX09AN57G. The National Center for Atmospheric Research is sponsored by the National Science Foundation.

[31] Robert Lysak thanks the reviewers for their assistance in evaluating this paper.

References

Anthes, R., et al. (2008), The COSMIC/FORMOSAT-3 mission: Early results, *Bull. Am. Meterol. Soc.*, *89*, 313–333.

Cheng, C.-Z. F., Y.-H. Kuo, R. A. Anthes, and L. Wu (2006), Satellite constellation monitors global and space weather, *Eos Trans. AGU*, *87*(17), 166.

Clilverd, M. A., A. J. Smith, and N. R. Thomson (1991), The annual variation in quiet time plasmaspheric electron density, determined from whistler mode group delays, *Planet. Space Sci.*, *39*, 1059–1067.

England, S. L., S. Maus, T. J. Immel, and S. B. Mende (2006), Longitudinal variation of the E-region electric fields caused by atmospheric tides, *Geophys. Res. Lett.*, *33*, L21105, doi:10.1029/2006GL027465.

England, S. L., T. J. Immel, J. D. Huba, M. E. Hagan, A. Maute, and R. DeMajistre (2010), Modeling of multiple effects of atmospheric tides on the ionosphere: An examination of possible coupling mechanisms responsible for the longitudinal structure of the equatorial ionosphere, *J. Geophys. Res.*, *115*, A05308, doi:10.1029/2009JA014894.

Fang, T.-W., H. Kil, G. Millward, A. D. Richmond, J.-Y. Liu, and S.-J. Oh (2009), Causal link of the wave-4 structures in plasma density and vertical plasma drift in the low-latitude ionosphere, *J. Geophys. Res.*, *114*, A10315, doi:10.1029/2009JA014460.

Forbes, J. M., X. Zhang, S. Palo, J. Russell, C. J. Mertens, and M. Mlynczak (2008), Tidal variability in the ionospheric dynamo region, *J. Geophys. Res.*, *113*, A02310, doi:10.1029/2007JA012737.

Forbes, J. M., S. L. Bruinsma, X. Zhang, and J. Oberheide (2009), Surface-exosphere coupling due to thermal tides, *Geophys. Res. Lett.*, *36*, L15812, doi:10.1029/2009GL038748.

Hagan, M. E., A. Maute, R. G. Roble, A. D. Richmond, T. J. Immel, and S. L. England (2007), Connections between deep tropical clouds and the Earth's ionosphere, *Geophys. Res. Lett.*, *34*, L20109, doi:10.1029/2007GL030142.

Hagan, M. E., A. Maute, and R. G. Roble (2009), Tropospheric tidal effects on the middle and upper atmosphere, *J. Geophys. Res.*, *114*, A01302, doi:10.1029/2008JA013637.

Hartman, W. A., and R. A. Heelis (2007), Longitudinal variations in the equatorial vertical drift in the topside ionosphere, *J. Geophys. Res.*, *112*, A03305, doi:10.1029/2006JA011773.

Häusler, K., H. Lühr, M. E. Hagan, A. Maute, and R. G. Roble (2010), Comparison of CHAMP and TIME-GCM nonmigrating tidal signals in the thermospheric zonal wind, *J. Geophys. Res.*, *115*, D00I08, doi:10.1029/2009JD012394.

He, M., L. Liu, W. Wan, J. Lei, and B. Zhao (2010), Longitudinal modulation of the O/N_2 column density retrieved from TIMED/GUVI measurement, *Geophys. Res. Lett.*, *37*, L20108, doi:10.1029/2010GL045105.

Huang, C.-S., F. J. Rich, O. de La Beaujardiere, and R. A. Heelis (2010), Longitudinal and seasonal variations of the equatorial ionospheric ion density and eastward drift velocity in the dusk sector, *J. Geophys. Res.*, *115*, A02305, doi:10.1029/2009JA014503.

Immel, T. J., E. Sagawa, S. L. England, S. B. Henderson, M. E. Hagan, S. B. Mende, H. U. Frey, C. M. Swenson, and L. J. Paxton (2006), Control of equatorial ionospheric morphology by atmospheric tides, *Geophys. Res. Lett.*, *33*, L15108, doi:10.1029/2006GL026161.

Jin, H., Y. Miyoshi, H. Fujiwara, and H. Shinagawa (2008), Electrodynamics of the formation of ionospheric wave number 4 longitudinal structure, *J. Geophys. Res.*, *113*, A09307, doi:10.1029/2008JA013301.

Kakinami, Y., C. H. Lin, J. Y. Liu, M. Kamogawa, S. Watanabe, and M. Parrot (2011), Daytime longitudinal structures of electron density and temperature in the topside ionosphere observed by the Hinotori and DEMETER satellites, *J. Geophys. Res.*, *116*, A05316, doi:10.1029/2010JA015632.

Kelley, M. C., V. K. Wong, N. Aponte, C. Coker, A. J. Mannucci, and A. Komjathy (2009), Comparison of COSMIC occultation-based electron density profiles and TIP observations with Arecibo incoherent scatter radar data, *Radio Sci.*, *44*, RS4011, doi:10.1029/2008RS004087.

Kil, H., R. DeMajistre, L. J. Paxton, and Y. Zhang (2006), Nighttime *F* region morphology in the low and middle latitudes seen from DMSP F15 and TIMED/GUVI, *J. Atmos. Sol. Terr. Phys.*, *68*, 1672–1681, doi:10.1026/j.jastp.2006.05.024.

Kil, H., E. R. Talaat, S.-J. Oh, L. J. Paxton, S. L. England, and S.-J. Su (2008), Wave structures of the plasma density and $\mathbf{E} \times \mathbf{B}$ drift in low-latitude F region, *J. Geophys. Res.*, *113*, A09312, doi:10.1029/2008JA013106.

Lei, J., et al. (2007), Comparison of COSMIC ionospheric measurements with ground-based observations and model predictions: Preliminary results, *J. Geophys. Res.*, *112*, A07308, doi:10.1029/2006JA012240.

Lin, C. H., W. Wang, M. E. Hagan, C. C. Hsiao, T. J. Immel, M. L. Hsu, J. Y. Liu, L. J. Paxton, T. W. Fang, and C. H. Liu (2007), Plausible effect of atmospheric tides on the equatorial ionosphere observed by the FORMOSAT-3/COSMIC: Three-dimensional electron density structures, *Geophys. Res. Lett.*, *34*, L11112, doi:10.1029/2007GL029265.

Liu, J. Y., C. Y. Lin, C. H. Lin, H. F. Tsai, S. C. Solomon, Y. Y. Sun, I. T. Lee, W. S. Schreiner, and Y. H. Kuo (2010), Artificial plasma cave in the low-latitude ionosphere results from the radio occultation inversion of the FORMOSAT-3/COSMIC, *J. Geophys. Res.*, *115*, A07319, doi:10.1029/2009JA015079.

Liu, L., M. He, W. Wan, and M.-L. Zhang (2008), Topside ionospheric scale heights retrieved from Constellation Observing System for Meteorology, Ionosphere, and Climate radio occultation measurements, *J. Geophys. Res.*, *113*, A10304, doi:10.1029/2008JA013490.

Liu, L., H. Le, Y. Chen, M. He, W. Wan, and X. Yue (2011), Features of the middle- and low-latitude ionosphere during solar minimum as revealed from COSMIC radio occultation measurements, *J. Geophys. Res.*, *116*, A09307, doi:10.1029/2011JA016691.

Luan, X., L. Liu, W. Wan, J. Lei, S.-R. Zhang, J. M. Holt, and M. P. Sulzer (2006), A study of the shape of topside electron density profile derived

from incoherent scatter radar measurements over Arecibo and Millstone Hill, *Radio Sci.*, *41*, RS4006, doi:10.1029/2005RS003367.

Lühr, H., M. Rother, K. Häusler, P. Alken, and S. Maus (2008), The influence of nonmigrating tides on the longitudinal variation of the equatorial electrojet, *J. Geophys. Res.*, *113*, A08313, doi:10.1029/2008JA013064.

McIlwain, C. E. (1961), Coordinates for mapping the distribution of magnetically trapped particles, *J. Geophys. Res.*, *66*(11), 3681–3691.

Millward, G. H., I. C. F. Muller-Wodarg, A. D. Aylward, T. J. Fuller-Rowell, A. D. Richmond, and R. J. Moffett (2001), An investigation into the influence of tidal forcing on F region equatorial vertical ion drift using a global ionosphere thermosphere model with coupled electrodynamics, *J. Geophys. Res.*, *106*, 24,733–24,744, doi:10.1029/2000JA000342.

Millward, G. H., A. D. Richmond, T. J. Fuller-Rowell, and A. D. Aylward (2007), Modeling the effects of changes in the terrestrial magnetic field on the climatology of the mid- and low-latitude ionosphere, *Eos Trans. AGU*, *88*(52), Fall Meet. Suppl., Abstract SA21B-08.

Oberheide, J., J. M. Forbes, K. Häusler, Q. Wu, and S. L. Bruinsma (2009), Tropospheric tides from 800 to 400 km: Propagation, interannual variability, and solar cycle effects, *J. Geophys. Res.*, *114*, D00I05, doi:10.1029/2009JD012388.

Oberheide, J., J. M. Forbes, X. Zhang, and S. L. Bruinsma (2011), Wave-driven variability in the ionosphere-thermosphere-mesosphere system from TIMED observations: What contributes to the "wave 4"?, *J. Geophys. Res.*, *116*, A01306, doi:10.1029/2010JA015911.

Pancheva, D., and P. Mukhtarov (2010), Strong evidence for the tidal control on the longitudinal structure of the ionospheric F-region, *Geophys. Res. Lett.*, *37*, L14105, doi:10.1029/2010GL044039.

Pedatella, N. M., and K. M. Larson (2010), Routine determination of the plasmapause based on COSMIC GPS total electron content observations of the midlatitude trough, *J. Geophys. Res.*, *115*, A09301, doi:10.1029/2010JA015265.

Pedatella, N. M., J. M. Forbes, and J. Oberheide (2008), Intra-annual variability of the low-latitude ionosphere due to nonmigrating tides, *Geophys. Res. Lett.*, *35*, L18104, doi:10.1029/2008GL035332.

Picone, J. M., A. E. Hedin, D. P. Drob, and A. C. Aikin (2002), NRLMSISE-00 empirical model of the atmosphere: Statistical comparisons and scientific issues, *J. Geophys. Res.*, *107*(A12), 1468, doi:10.1029/2002JA009430.

Ren, Z., W. Wan, L. Liu, B. Zhao, Y. Wei, X. Yue, and R. A. Heelis (2008), Longitudinal variations of electron temperature and total ion density in the sunset equatorial topside ionosphere, *Geophys. Res. Lett.*, *35*, L05108, doi:10.1029/2007GL032998.

Richmond, A. D. (1995), Ionospheric electrodynamics using magnetic apex coordinates, *J. Geomagn. Geoelectr.*, *47*, 191–212.

Richmond, A. D., E. C. Ridly, and R. G. Roble (1992), A thermosphere/ionosphere general circulation model with coupled electrodynamics, *Geophys. Res. Lett.*, *19*(6), 601–604, doi:10.1029/92GL00401.

Rocken, C., Y.-H. Kuo, W. Schreiner, D. Hunt, S. Sokolovskiy, and C. McCormick (2000), COSMIC system description, *Terr. Atmos. Ocean Sci.*, *11*, 21–52.

Sagawa, E., T. J. Immel, H. U. Frey, and S. B. Mende (2005), Longitudinal structure of the equatorial anomaly in the nighttime ionosphere observed by IMAGE/FUV, *J. Geophys. Res.*, *110*, A11302, doi:10.1029/2004JA010848.

Scherliess, L., D. C. Thompson, and R. W. Schunk (2008), Longitudinal variability of low-latitude total electron content: Tidal influences, *J. Geophys. Res.*, *113*, A01311, doi:10.1029/2007JA012480.

Schunk, R. W., and A. F. Nagy (2000), *Ionospheres: Physics, Plasma Physics, and Chemistry*, Cambridge Univ. Press, New York.

Su, Y. Z., K.-I. Oyama, G. J. Bailey, S. Fukao, T. Takahashi, and H. Oya (1996), Longitudinal variations of the topside ionosphere at low latitudes: Satellite measurements and mathematical modelings, *J. Geophys. Res.*, *101*(A8), 17,191–17,205.

Talaat, E. R., and R. S. Lieberman (2010), Direct observations of nonmigrating diurnal tides in the equatorial thermosphere, *Geophys. Res. Lett.*, *37*, L04803, doi:10.1029/2009GL041845.

Titheridge, J. E. (1998), Temperatures in the upper ionosphere and plasmasphere, *J. Geophys. Res.*, *103*(A2), 2261–2277.

Tulasi Ram, S., C. H. Liu, S.-Y. Su, and R. A. Heelis (2010), A comparison of ionospheric O+/light-ion transition height derived from ion-composition measurements and the topside ion density profiles over equatorial latitudes, *Geophys. Res. Lett.*, *37*, L20107, doi:10.1029/2010GL045199.

Wan, W., L. Liu, X. Pi, M. L. Zhang, B. Ning, J. Xiong, and F. Ding (2008), Wavenumber-4 patterns of the total electron content over the low latitude ionosphere, *Geophys. Res. Lett.*, *35*, L12104, doi:10.1029/2008GL033755.

Wan, W., J. Xiong, Z. Ren, L. Liu, M.-L. Zhang, F. Ding, B. Ning, B. Zhao, and X. Yue (2010), Correlation between the ionospheric WN4 signature and the upper atmospheric DE3 tide, *J. Geophys. Res.*, *115*, A11303, doi:10.1029/2010JA015527.

Watanabe, S., and K. I. Oyama (1996), Effects of neutral wind on the electron temperature at a height of 600 km in the low latitude region, *Ann. Geophys.*, *14*, 290–296.

Yue, X., W. S. Schreiner, J. Lei, S. V. Sokolovskiy, C. Rocken, D. C. Hunt, and Y.-H. Kuo (2010), Error analysis of Abel retrieved electron density profiles from radio occultation measurements, *Ann. Geophys.*, *28*, 217–222, doi:10.5192/angeo-28-217-2010.

T.-W. Fang and G. Millward, Space Weather Prediction Center, NOAA, 325 Broadway, Boulder, CO 80305, USA. (tzu-wei.fang@noaa.gov; george.millward@noaa.gov)

J. M. Forbes and K. M. Larson, Department of Aerospace Engineering Sciences, University of Colorado at Boulder, 429 UCB, Boulder, CO 80309, USA. (forbes@colorado.edu; kristinem.larson@gmail.com)

A. Maute, N. M. Pedatella, and A. D. Richmond, High Altitude Observatory, National Center for Atmospheric Research, PO Box 3000, Boulder, CO 80307-3000, USA. (maute@ucar.edu; nicholas.pedatella@colorado.edu; richmond@ucar.edu)